Microscopic description of flow defects and relaxation in metallic glasses

M. Atzmon[1,2,*] and J. D. Ju[2]

[1]*Department of Nuclear Engineering and Radiological Sciences, University of Michigan, Ann Arbor, Michigan 48109, USA*

[2]*Department of Materials Science and Engineering, University of Michigan, Ann Arbor, Michigan 48109, USA*

(Received 26 October 2012; revised manuscript received 31 July 2014; published 29 October 2014)

The anelastic relaxation behavior of amorphous $Al_{86.8}Ni_{3.7}Y_{9.5}$ was characterized in prolonged, quasistatic measurements, up to 1.1×10^8 s. The size-density distribution of *potential* shear transformation zones was determined from the data. We derive an expression for the distribution, based on a free-volume criterion for an atomic cluster being a *potential* shear transformation zone. The model is shown to be consistent with experiment.

DOI: 10.1103/PhysRevE.90.042313 PACS number(s): 46.35.+z, 81.40.Jj, 62.40.+i, 83.60.Bc

I. INTRODUCTION

Atomic transport in glasses has long posed challenges to researchers. In analogy to crystalline solids, transport processes are believed to be mediated by structural defects. However, because the atomic-scale structure of glasses is ill defined, there is no straightforward way of defining defects in them. Moreover, unlike for crystalline materials, there is no known contrast mechanism that would allow for direct imaging of such defects. Also in contrast to crystalline solids, because of the nonequilibrium state of glasses, they undergo thermally activated densification. As a result, the rates of transport-limited processes, e.g., diffusion or flow, are known to decrease by orders of magnitude with structural relaxation [1]. This correlation and Ref. [2] indicate the existence of structural defects associated with the free volume (FV). Cohen and Turnbull analyzed atomic diffusion in glasses in terms of vacancylike defects [3]. Spaepen [4] later derived a constitutive model for metallic glasses based on the same model. The present work is based on later insights that flow defects in metallic glasses are extended and not vacancylike.

Two-dimensional bubble rafts [5] and three-dimensional colloidal suspensions [6], used as physical analogs, and molecular dynamics simulations [7–9] indicate that flow in a metallic glass is accommodated by shear transformations of equiaxed clusters of atoms, the surroundings of which deform elastically. At low strain, these shear transformation zones (STZs) are isolated. Upon removal of the external constraint, back stress in the surrounding, elastic, matrix can lead to reversal, i.e., to anelastic behavior [10,11]. At high strain, and therefore large volume fraction occupied by STZs, back stress is lost and deformation is permanent. Building on Spaepen's activated-state rate theory for vacancylike defects [4], Argon [12] expressed the shear strain rate due to STZs of volume Ω under a net shear stress σ_s:

$$\dot{\gamma} = 2c\gamma_0^c \nu_G \exp\left(-\Delta F/kT\right) \sinh\left(\sigma_s \gamma_0^T \Omega/2kT\right), \quad (1)$$

where ν_G is the attempt frequency, kT has its usual meaning, γ_0^T is the unconstrained shear strain in the saddle-point configuration, and γ_0^c is the value under constraint by the elastic matrix. c is the volume fraction occupied by *potential* STZs: A *potential* STZ (PSTZ), also previously termed "fertile region" [13], is a cluster of atoms capable of undergoing dissipative shear and thus becoming an STZ. In this treatment, a single STZ size was implicitly assumed. When STZs occupy a small volume fraction and are therefore isolated, ΔF is dominated by elastic strain around the STZ and given by [14,15]

$$\Delta F = \left\{\left[\frac{(7-5\nu)}{30(1-\nu)} + \frac{2(1+\nu)}{9(1-\nu)}\bar{\beta}^2\right]\gamma_0^T + \frac{1}{2}\frac{\bar{\sigma}_{STZ}}{\mu}\right\}\mu\gamma_0^T\Omega, \quad (2)$$

where ν is Poisson's ratio, $\bar{\beta}^2 \sim 1$ the dilatancy factor, $\mu = E_0/[2(1+\nu)]$, the shear modulus, E_0, Young's modulus, and $\bar{\sigma}_{STZ}$ the shear resistance of the STZ. Equation (2) is dominated by the total elastic strain energy due to shear and dilatation, expressed by the first two terms on the right-hand side, respectively [15]. These terms include contributions from both the STZ and the surrounding matrix.

Argon and Kuo [10] used anelastic recovery measurements, coupled with temperature stepping, to obtain an approximate spectrum of activation free energies for shear transformations. They argued that the width of this spectrum is a reflection of the distribution of FV. Bouchbinder and Langer [16] have analyzed the anelastic response of a glass by postulating an exponential distribution of activation barriers. They added a smoothed cutoff for the upper limit on the activation barrier, since in the flow regime in which the population of potential STZs is continually regenerated there is an upper limit on relaxation times. In contrast, in the regime we explore, the population of potential STZs is fixed, as evidenced by the complete reversibility of strain [17]. Therefore, any observed upper limit on the activation barrier and relaxation times is likely due to experimental conditions, as discussed below.

There is a significant body of literature on advanced stages of plasticity in metallic glasses, including catastrophic failure by flow localization [18]. In this regime, PSTZs are created and annihilated continually. However, for the same reason that plasticity studies in crystalline metals required detailed investigations of dislocation behavior, a full understanding of the dynamics of isolated STZs is required. Such an understanding has been incomplete. Atomistic simulations [7–9] have provided important insights, but these cannot fully capture thermally activated, and therefore rare, shear transformations under realistic conditions.

We have recently observed the time-dependent component of room-temperature deformation in amorphous $Al_{86.8}Ni_{3.7}Y_{9.5}$ after constraining for 2×10^6 s to be fully

*Author to whom correspondence should be addressed: atzmon@umich.edu

reversible. The strain was kept low so as to obtain isolated STZs. We identified a signature of isolated STZs [17]: The spectrum of time constants, calculated from the corresponding quasistatic anelastic relaxation data, consisted of distinct peaks centered at τ_n.[1] These were analyzed based on a standard linear solid model [19], generalizing Eq. (1) to include contributions to the strain rate, $\dot{\gamma}_n$, by each n-type STZ as a function of the respective c_n, Ω_n, and ΔF_n. To a great degree of agreement, $\Omega_n = n\Omega_0$, where Ω_0 is the atomic volume of Al, the majority element. We thus demonstrated an atomically quantized hierarchy of STZs, ranging in size from $n = 14$ to 21 atoms, with correspondingly increasing time constants. Smaller STZs were too fast and few to be measured, whereas larger PSTZs were frozen for the given time and temperature. The fact that a single element, Al, constitutes nearly 90% of the alloy likely facilitated the resolution of the atomically quantized volume increments. Since $\Delta F_n \propto \Omega_n$, this hierarchy provides a straightforward interpretation of the distribution of activation free energies observed by Argon and Kuo [10]. Because of inherent resolution limits imposed by the temperature-stepping method they employed, they did not resolve peaks in the distribution. We have recently obtained similar results from dynamic moduli of a different metallic glass [20], suggesting that our model is valid for a range of alloys.

Most importantly, we obtained in Ref. [17] the size-density distribution of PSTZs, c_n. It is the total volume occupied by PSTZs of size n per unit volume, counting overlapping volumes multiple times. The mechanical reversibility we observed is consistent with the fact that the fraction of PSTZs that have transformed is small, so they are isolated and can thus be reversed by the back stress in the undeformed matrix [10,11]. The detailed c_n data are of crucial importance in the search for answers to fundamental questions about glass behavior. For example, no quantitative criterion has been articulated to date that determines whether an atomic cluster in a metallic glass can undergo dissipative shear, i.e., whether it is a PSTZ. Any such criterion would need to incorporate the role of structural relaxation.

In the present work, significantly longer constraining times and subsequent relaxation times were employed than in Ref. [17], for the same alloy. The results are consistent with Ref. [17] for $n = 14, \ldots, 20$, but provide more reliable data for STZs comprising 21 atoms. In Ref. [17], the latter had not reached mechanical equilibrium during the constraining period, so that c_{21} had to be estimated by extrapolation. STZs with $n = 22$, predicted in Ref. [17], also contribute to the present data. We present an expression for the size-density distribution of PSTZs, based on an FV criterion we postulate. It is shown to be consistent with the data. We also compare the STZ spectrum in the as-quenched state with those following structural relaxation: Relaxation reduces the number of PSTZs, but preserves their properties.

[1] In Ref. [17], the peaks were labeled with $m = 1, \ldots, 8$. The index $n = 13 + m$ used here refers to the number of atoms comprised by an STZ, as detailed below.

II. EXPERIMENT AND ANALYSIS

An amorphous $Al_{86.8}Ni_{3.7}Y_{9.5}$ ribbon, 22 μm thick and 1 mm wide, was obtained by single-wheel melt spinning. Electron diffraction analyses were employed to confirm the amorphous structure before and after structural relaxation (3600 s at 110°C). The strain vs time during anelastic relaxation at 295 $\pm$ 1 K was characterized by a combination of (a) cantilever measurements of the displacement under fixed load, with an Agilent G200 nanoindenter with a DCM head, for 1–200 s (three to four samples of each type, 70–95 measurements for each) and (b) bend-stress relaxation ("mandrel") measurements of the radius of curvature during stress-free relaxation for durations up to 1.1×10^8 s, following constraining at fixed radius for 4.4×10^7 s (as-quenched, two samples), and 2×10^6 s (as-quenched and relaxed, five to six samples each). For the mandrel method, the maximum elastic strain, attained at the surface, was below 0.3%, i.e., well below yield, and the anelastic strain was below 0.12%. For the cantilever method, the values were far lower. For details, see Ref. [17]. The spectrum of time constants for exponential anelastic relaxation, $f(\tau)$, was determined by nonlinear least-squares fit [17,21]. Significant effort was expended to verify the independence of the analysis results of initial guesses, choice of interval width or number of points, and the method was validated with simulated data that included noise. Unlike with the commonly assumed phenomenological stretched-exponential behavior, $\exp[-(t/\tau)^b]$ [22,23], where t is the time and τ, b are constants, the spectrum was obtained directly without making any assumption on its shape. The anelastic component of the bending strain under constraint at mechanical equilibrium, associated with peak n in $f(\tau)$, is given by [17]

$$\varepsilon_n^0 = \varepsilon_{el}^0 \int_n f(\tau) d \ln \tau, \tag{3}$$

with integration over the respective peak, where ε_{el}^0 is the elastic bending strain at mechanical equilibrium.

III. RESULTS AND DISCUSSION

In Fig. 1, the anelastic strain at the surface, normalized by the equilibrium elastic strain, is displayed as a function of time for stress-free samples following constraint at two different strains for 4.4×10^7 s. A sample curve obtained $\leq$200 s by the cantilever method is reproduced from Ref. [17]. Because the mandrel constraining time was longer than in Ref. [17], the data also include a contribution from STZs comprising 22 atoms, associated with a time constant of $\tau_{22} = 1.68 \times 10^8$ s, as extrapolated from Ref. [17]. However, as the duration of the stress-free relaxation is much shorter than τ_{22}, the unrecovered anelastic strain is still large at the end of the measurement, and the corresponding peak in $f(\tau)$ is not fully obtained. This part of the data confirms our earlier assumption that the observed STZ size range was part of a broader hierarchy.

The observed linearity of the anelastic strain in the elastic strain in Fig. 1, and therefore in the stress, supports the assumption of a neutral midplane in the determination of the strain from the radius of curvature. It also supports fitting the solid as a spring and several Voigt units in series (Fig. 2).

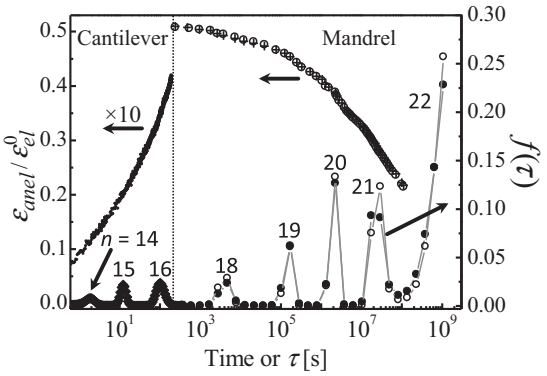

FIG. 1. Representative normalized anelastic strain vs time curves under fixed stress (cantilever experiment [17]) and stress-free (mandrel experiment after constraining for 4.4×10^7 s) for as-quenched samples. For the former, "×10" indicates that the values displayed are ten times the measured values. For the latter, data were obtained for two radii and corresponding elastic strain at mechanical equilibrium, $\varepsilon_{el}^0 = 0.184\%$ (+) and 0.237% (open circles). The relaxation-time spectra, $f(\tau)$ (filled and open circles, respectively, for the mandrel experiments), are computed from these curves [17,21]. The integer peak index, n, was selected to reflect the fact that it is approximately equal to Ω_n/V_{Al} (see Fig. 2).

Each Voigt unit is responsible for one spectrum peak and consists of a spring and dashpot in parallel, with effective modulus E_n' and effective viscosity η_n', respectively. The volume fraction occupied by PSTZs of size n is given by [17]

$$c_n = E_0/E_n' = \varepsilon_n^0/\varepsilon_{el}^0 = \int_n f(\tau) d \ln \tau \qquad (4)$$

(Fig. 3), where E_0 is the high-frequency Young's modulus, 48.2 GPa [24]. This relationship is based on the determination that the STZs are at internal equilibrium, so that the ensemble-averaged strain of all n-size STZs is equal to the time-averaged strain of each n-size STZ. Equation (4), based on mechanical equilibrium, allows for a highly reliable determination of c_n, in contrast to the notoriously large error bars typical of preexponential factors obtained from kinetic data. Since overlapping PSTZs are counted multiple times, $c_n > 1$ is possible, which merely means that the anelastic strain may be greater than the elastic strain. At the low anelastic strains of the experiment, however, only a small fraction of the PSTZs have transformed. The volume fraction occupied by the elastic matrix is therefore essentially 100% and strain independent, and so is E_0.

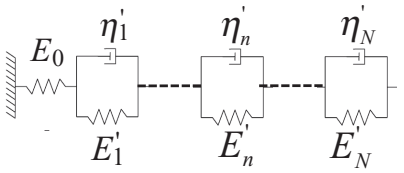

FIG. 2. Linear solid model: N anelastic units act in series, where n-type sites are associated with Young's modulus of E_n' and viscosity η_n', both effective quantities that are inversely proportional to the volume fraction occupied by these sites.

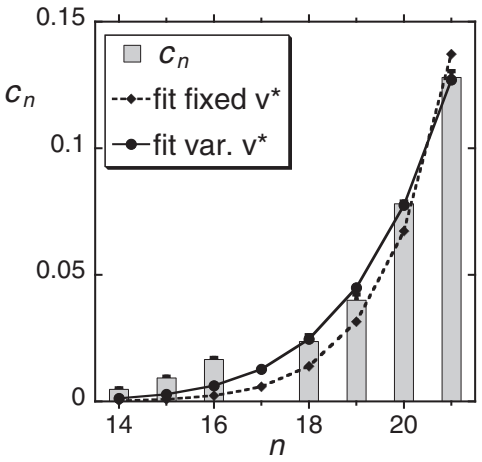

FIG. 3. Size-density distribution of STZs, c_n as a function of n, calculated from the data (bars) and fitted with c_n^{model} from Eqs. (5) and (6) (curves) with fixed or variable v^*. The lines are guides to the eye.

In order to validate the model for the present data, $\eta_n' = \tau_n E_n'/3$ and Ω_n were calculated for each spectrum peak, n, using Eqs. (1) and (2). For each sample type, the values were averaged over individual measurements. The random error was estimated as the standard deviation of the mean. The STZ volume, Ω_n, normalized by that of an Al atom is linear in n with a slope within <5% of unity, similar to Ref. [17], confirming again the designation of n as the number of atoms in an STZ.

In contrast to the uncertainty in c_{21} in Ref. [17] due to a correction for the short constraining time of 2×10^6 s, the data in Fig. 3 are reliable up to $n = 21$, and provide an unprecedented opportunity to shed light on the nature of flow defects in a metallic glass. In particular, they can be used to examine possible criteria that define what renders an equiaxed atomic cluster a PSTZ. The following discussion is based on the FV model, but may also account for alternative models of flow defects that obey Poisson statistics. Since atomic rearrangements require sufficient local FV, prior analyses based on vacancylike defects [3,4] assumed the rate of diffusion or flow to be proportional to the fraction of atomic sites at which the FV exceeds a set value, v^*, given by $\exp(-\gamma v^*/v_f)$ (Cohen and Turnbull [3]),where v_f is the average FV per atom and $\gamma \approx 1/2$ is a geometric factor.

The role of the FV in shear transformations will now be discussed. We argued in Ref. [17] that, in contrast to Argon and Kuo's conclusion [5], the range of $\Delta F_n \propto \Omega_n \propto n$ values rules out a significant contribution of the FV to the *width* of the ΔF spectrum. While a cluster being a PSTZ requires that it contain sufficient FV, ΔF_n is averaged over the long-range elastic field [12,14,15] and is not sensitive to FV fluctuations. The observation below that structural relaxation only affects c_n, but not the size histogram, further confirms our interpretation.

One might tentatively argue that for an atomic cluster to be a PSTZ, the FV associated with *each* of its atoms needs to exceed a set value. However, it is easy to show that the probability of satisfying such a requirement decreases sharply with cluster size, opposite to the trend in Fig. 3. Assuming that FV can be

shared dynamically among the atoms that make up a cluster during a time scale shorter than that required to overcome ΔF_n, the following is therefore postulated: An atomic cluster of size n is a PSTZ if the *total* FV it contains exceeds a set value, v^*, that is only weakly dependent on n. Defining $g(n)$ as the number of near-equiaxed clusters of size n, centered at a given atom, the number per atom of such clusters is derived from the Cohen-Turnbull expression [3]:

$$N_n(v^*) = g(n)\int_{v_1+\cdots+v_n>v^*} dv_1\cdots dv_n \left\{(\gamma/v_f)^n \times \prod_{i=1}^{n}\exp[-(\gamma v_i/v_f)]\right\} = g(n)\left(\sum_{i=0}^{n-1}\frac{1}{i!}(\gamma v^*/v_f)^i\right)\exp(-\gamma v^*/v_f). \quad (5)$$

The predicted c_n is given by

$$c_n^{\text{model}} = nN_n(v^*), \quad (6)$$

which approaches $ng\,(n)$ for large n. It is important to note that while high-n PSTZs may be abundant since they contain sufficient FV, they are frozen at temperatures below T_g because of the high barrier, $\Delta F_n \propto \Omega_n \propto n$, associated with the long-range elastic field.

In Fig. 3, a fit of c_n^{model} to the data is shown, with $\gamma v^*/v_f$ as the only fitting parameter, approximating it as independent of n. We assume $g\,(n) = 5$ for all n. The best fit yields $\gamma v^*/v_f = 38.8$. It agrees with the trend in the data, but underestimates c_n at small n. This suggests a dependence of v^* on n. Therefore, the c_n data were refitted (included in Fig. 3) with v^* obeying a power-law dependence on n:

$$\gamma v^*/v_f = \alpha n^\beta, \quad (7)$$

where α and β are dimensionless fitting parameters. The best fit yields $\alpha = 19.9$ and $\beta = 0.22$. The small-n values are still overestimated, but to a lesser extent. These are values obtained from the cantilever experiments at fixed stress—the discrepancy may be due to an unknown systematic difference between the methods used for the two time regimes. The small value of β indicates a mild variation of the threshold v^*, in agreement with the assumption. If v^* varied as the linear dimension of the PSTZ, i.e., with the required migration distance for FV redistribution, $\beta = 1/3$ would be obtained. The range of $\gamma v^*/v_f$ values, 36–39, indicates that a PSTZ has at least ~four times the average FV *per atom* in this STZ size range. These values are about twice those in Ref. [25], but a direct comparison is not meaningful because the latter uses a vacancylike model.

Anelastic relaxation measurements have also been conducted with structurally relaxed samples. The shorter constraining time used, 2×10^6 s, did not allow a comparison with the c_n data of Fig. 3. However, comparison of data before and after structural relaxation for the same constraining time shows that Ω_n, and therefore the corresponding ΔF_n, remain the same within 1% following structural relaxation. For the degree of relaxation used, only minor changes in the elastic constants, and therefore on the activation barriers,

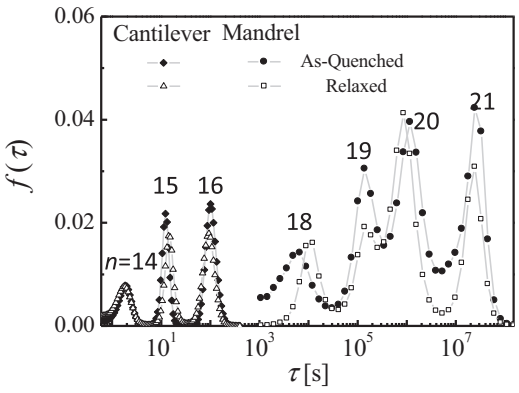

FIG. 4. Relaxation-time spectra for as-quenched and structurally relaxed samples following constraint for 2×10^6 s, indicating a decrease in the number of PSTZs upon structural relaxation.

are expected [26,27]. In Fig. 4, the relaxation-time spectra before and after structural relaxation, following constraint duration of 2×10^6 s, are shown. The peak areas decrease upon structural relaxation, indicating a decrease of c_n [Eq. (4)]. These observations indicate that relaxation affects the number of PSTZs, but not their properties. This is a generalization of Taub and Spaepen's conclusion from flow data in a metallic glass, for which the single apparent activation energy for flow was independent of structural relaxation [25].

The fit of c_n^{model} to the data, while imperfect, suggests a change in FV of ~3% upon structural relaxation. Again, a direct comparison with the numbers in Ref. [25] cannot be made. It would be important to examine the present results in future densification studies with varying degrees of structural relaxation. It should be noted that $Al_{86.8}Ni_{3.7}Y_{9.5}$ is a marginal glass former. While it does not crystallize during plastic deformation [28], its resistance to thermally activated crystallization is poor. Therefore, the range of experimentally accessible structural-relaxation states and associated FV values is narrow, and it would be instructive to apply the present methodology in the future to more-stable metallic glasses. In Ref. [25], for example, a wider range of viscosities is observed as a function of relaxation state. We point out that Ref. [29] reports conclusions different from ours regarding the effect of relaxation. However, it relies on a method [30] that suffers from several artifacts and therefore drastically overestimates the STZ size [17].

Unlike the present approach, other studies have only yielded a dominant STZ size, which depends on the temperature range of the experiment. The present anelasticity-based approach resolves a range of PSTZ sizes. Above this range, ΔF_n is high, and thermal fluctuations of this magnitude are rare. Below this range, the transformation rate may be too high to resolve, or the volume fraction, $\phi = [1 - \exp(-c_n)]$, too low. In contrast to anelastic measurements, there is no known reliable way of obtaining basic STZ properties from macroscopic flow experiments since irreversible deformation involves larger-scale atomic transport, during which STZs interact with each other and new PSTZs form. The great advantage of the present work is that it provides size-resolved properties of STZs. These allow for extrapolation to larger sizes, for which c_n is sufficiently large to dominate observed phenomena [20]. For example, a necessary condition for flow

initiation is that the rigid volume fraction of the solid, *not* occupied by thermally activated PSTZs, $1-\phi$, be lower than the percolation threshold [31].

Another phenomenon that is possibly mediated by STZs is long-range atomic diffusion: It would require ϕ to exceed the percolation threshold. In earlier work by one of the authors [32], the effective diffusion coefficient in a compositionally modulated amorphous alloy was observed to decrease sharply from an initially high value. This behavior is consistent with an STZ-based mechanism for which the diffusion coefficient is initially high due to activity of small STZs, which have a low activation barrier. Once these are exhausted, subsequent mixing requires larger STZs, which are slower.

If the size of an STZ is larger than that of the triggering cluster [13,33], our results provide the latter to a good approximation, since it appears in the exponent in Eq. (1) and in its generalization to multiple sizes [17]. Recently, Fan *et al.* [33] computed the activation energies for shear transformations using the activation-relaxation technique in an unstressed glass. Our experiments are in a similar regime, since the small stresses induce only small perturbations on thermal fluctuations. Similar to our result, Fan *et al.* show that the properties of triggering clusters are independent of the state of structural relaxation—only the distribution varies. Their triggering clusters are smaller than ours, consisting of fewer than ten atoms. For this small STZ size, one would expect from the Eshelby theory [14] and Eq. (2) a lower activation energy than the values of ~1–2 eV in Ref. [33]. We attribute this small size to possible differences in the displacement field between experiment and simulation. One possibility is that the saddle point determined in simulation leads to a shallow minimum and a subsequent increase in energy with displacement, i.e., implying a larger effective triggering cluster.

We have recently shown [34] that both alpha and beta relaxations can be described by the same STZ mechanism. The alpha relaxation is associated with the glass transition and is treated in the literature as irreversible (e.g., Ref. [33]). We argue that for sufficiently small strains, the large STZs, to which we attribute alpha relaxations, can be isolated so that the shear transformations are mechanically reversible due to back stress in the surrounding matrix.

IV. CONCLUSION

In conclusion, a theoretical expression for the size-density distribution of PSTZs in a metallic glass is proposed, which agrees with recently obtained, detailed data. Structural relaxation reduces the number of PSTZs, but leaves their properties essentially unchanged: While a sufficient amount of FV is required for a cluster of atoms to be a PSTZ, the activation barrier for a shear transformation, which is dominated by the long-range elastic field, is affected by structural relaxation only in a minor way, due to changes in the elastic moduli. These results represent a crucial step toward a full understanding of relaxation and atomic transport in metallic glasses. Further application and refinement of the methodology employed in this paper will likely lead to greater insights.

ACKNOWLEDGMENTS

This work was partly funded by the U.S. National Science Foundation (NSF), Grant No. DMR-1307884. The authors are grateful to Professor F. Spaepen (Harvard) and Professor A. L. Greer (Cambridge) for useful discussions, Dr. Dongchan Jang (KAIST) for nanoindenter measurements, and Dr. F. Pinkerton (General Motors) for sample preparation.

[1] F. Spaepen and A. I. Taub, in *Amorphous Metallic Alloys*, edited by F. E. Luborsky (Butterworths, London, 1983), Chap. 13, p. 231.
[2] H. S. Chen, J. Appl. Phys. **49**, 3289 (1978); A. L. Greer (private communication).
[3] M. H. Cohen and D. Turnbull, J. Chem. Phys. **31**, 1164 (1959).
[4] F. Spaepen, Acta Metall. **25**, 407 (1977).
[5] A. S. Argon and H. Y. Kuo, Mater. Sci. Eng. **39**, 101 (1979).
[6] P. Schall, D. A. Weitz, and F. Spaepen, Science **318**, 1895 (2007).
[7] M. L. Falk and J. S. Langer, Phys. Rev. E **57**, 7192 (1998).
[8] F. Delogu, Phys. Rev. Lett. **100**, 075901 (2008).
[9] M. Neudecker and S. G. Mayr, Acta Mater. **57**, 1437 (2009).
[10] A. S. Argon and H. Y. Kuo, J. Non-Cryst. Solids **37**, 241 (1980).
[11] E. Orowan, in *Proceedings of the First U.S. National Congress of Applied Mechanics, Chicago, Illinois, June 11–16, 1951* (ASME, New York, 1952), p. 453.
[12] A. S. Argon, Acta Metall. **27**, 47 (1979).
[13] A. S. Argon and M. J. Demkowicz, Metall. Mater. Trans. A **39**, 1762 (2008).
[14] J. D. Eshelby, Proc. R. Soc. A **241**, 376 (1957).
[15] A. S. Argon and L. T. Shi, Acta Metall. **31**, 499 (1983).
[16] E. Bouchbinder and J. S. Langer, Phys. Rev. Lett. **106**, 148301 (2011).
[17] J. D. Ju, D. Jang, A. Nwankpa, and M. Atzmon, J. Appl. Phys. **109**, 053522 (2011).
[18] A. L. Greer, Y. Q. Cheng, and E. Ma, Mater. Sci. Eng., R **74**, 71 (2013).
[19] C. Zener, *Elasticity and Anelasticity of Metals* (University of Chicago Press, Chicago, 1948), p. 43.
[20] J. D. Ju and M. Atzmon, Acta Mater. **74**, 183 (2014).
[21] J. R. Cost, J. Appl. Phys. **54**, 2137 (1983).
[22] R. Kohlrausch, Ann. Phys. (Leipzig, Ger.) **167**, 179 (1854).
[23] K. L. Ngai, J. Non-Cryst. Solids **275**, 7 (2000).
[24] J. M. Freitag, R. G. Koknaev, R. Sabet-Sharghi, M. Koknaeva, and Z. Altounian, J. Appl. Phys. **79**, 3967 (1996).
[25] A. I. Taub and F. Spaepen, Acta Metall. **28**, 1781 (1980).
[26] T. Ichitsubo, S. Kai, H. Ogi, M. Hirao, and K. Tanaka, Scr. Mater. **49**, 267 (2003).
[27] V. Keryvin, T. Rouxel, M. Huger, and L. Charleux, J. Ceram. Soc. Jpn. **116**, 851 (2008).
[28] W. H. Jiang, F. E. Pinkerton, and M. Atzmon, J. Mater. Res. **20**, 696 (2005).
[29] D. Pan, Y. Yokoyama, T. Fujita, Y. H. Liu, S. Kohara, A. Inoue, and M. W. Chen, Appl. Phys. Lett. **95**, 141909 (2009).
[30] D. Pan, A. Inoue, T. Sakurai, and M. W. Chen, Proc. Natl. Acad. Sci. USA **105**, 14769 (2008).

[31] C. D. Lorenz and R. M. Ziff, J. Chem. Phys. **114**, 3659 (2001).

[32] M. Atzmon and F. Spaepen, in *Science and Technology of Rapidly Quenched Alloys*, Materials Research Society Symposia Proceedings, Vol. 80, edited by W. L. Johnson, L. E. Tanner, and M. Tenhover (Materials Research Society, Pittsburgh, PA, 1987), pp. 55–59.

[33] Y. Fan, T. Iwashita, and T. Egami, Nat. Commun. **5**, 5083 (2014).

[34] J. D. Ju and M. Atzmon, MRS Commun. **4**, 63 (2014).